Journal of Sound and Vibration (2001) **247**(2), 325–341
doi:10.1006/jsvi.2001.3751, available online at http://www.idealibrary.com on IDEAL®

MODAL IDENTIFICATION OF TSING MA BRIDGE BY USING IMPROVED EIGENSYSTEM REALIZATION ALGORITHM

Q. Qin, H. B. Li and L. Z. Qian

Department of Civil Engineering, Tsinghua University, Beijing 100084, *People's Republic of China.*
E-mail: qq-dci@tsinghua.edu.cn

AND

C.-K. Lau

Civil Engineering Department, Government of Hong Kong SAR, Kowloon, Hong Kong

(*Received* 24 *July* 2000, *and in final form* 23 *April* 2001)

This paper presents the results of research work on modal identification of Tsing Ma bridge ambient testing data by using an improved eigensystem realization algorithm. The testing was carried out before the bridge was open to traffic and after the completion of surfacing. Without traffic load, ambient excitations were much less intensive, and the bridge responses to such ambient excitation were also less intensive. Consequently, the bridge responses were significantly influenced by the random movement of heavy construction vehicles on the deck. To cut off noises in the testing data and make the ambient signals more stationary, the Chebyshev digital filter was used instead of the digital filter with a Hanning window. Random decrement (*RD*) functions were built to convert the ambient responses to free vibrations. An improved eigensystem realization algorithm was employed to improve the accuracy and the efficiency of modal identification. It uses cross-correlation functions of *RD* functions to form the Hankel matrix instead of *RD* functions themselves and uses eigenvalue decomposition instead of singular value decomposition. The data for response accelerations were acquired group by group because of limited number of high-quality accelerometers and channels of data loggers available. The modes were identified group by group and then assembled by using response accelerations acquired at reference points to form modes of the complete bridge. Seventy-nine modes of the Tsing Ma bridge were identified, including five complex modes formed in accordance with unevenly distributed damping in the bridge. The identified modes in time domain were then compared with those identified in frequency domain and finite element analytical results.

1. INTRODUCTION

This paper discusses modal identification of the Tsing Ma bridge in time domain from ambient acceleration response data. The global dynamic characteristics such as natural frequencies, mode shapes and modal damping ratios are important for the seismic and wind resistance design, structural health monitoring and damage detection of bridges [1]. The Tsing Ma bridge with 1377 m main span is the longest suspension bridge carrying both road and rail traffic in the world. The bridge has been designed to carry a dual three-lane expressway on the upper deck and two railway tracks on the lower deck. The bridge deck is a continuous steel truss deck 2160 m in length, and the reinforced concrete towers, with

0022-460X/01/420325 + 17 $35.00/0

larger material damping than that of all of the welded steel stiffening deck, are 206 m high. Ambient vibration testing was selected because a large number of very powerful equipment is required to excite the 180,000 t of the bridge structure (which includes main cables, deck and pylons) for forced vibration testing and the requirement of normal traffic should not be affected for real-time health monitoring [2]. In order to establish initial signatures for future structural health monitoring, the ambient vibration measurement was carried out immediately after the completion of road surfacing, but before opening to traffic (the period between April 31 and May 28, 1997).

Different from previous testings on other suspension bridges (for instance, the Golden Gate bridge [3], Humber bridge, the second Bosporus bridge and so on), this testing was carried out prior to opening it to traffic. The ambient excitation on the Tsing Ma bridge, therefore, did not include traffic loads, the largest ambient load that made the acquired bridge responses relatively weak. Construction vehicles, especially heavy locomotives, randomly and temporarily moved on the deck during the testing, which strongly affected the bridge responses. These made the acquired responses non-stationary with low ratios of signal to noise. Both the low-pass digital filter based on the use of a Hanning window or others to truncate impulsive responses and obtain the spectral shaping [4] and analogue filter could not pre-process these signals effectively. Consequently, it was necessary for modal identification in this study to choose an effective digital filter. The Chebyshev digital filter developed in the 1970s could strictly define the passband edge and the stopband edge frequencies [4] and was considered most appropriate as a replacement of the digital filters with a Hanning window or other windows in this study.

Modal identification techniques in time domain need neither very large sampling length nor repeated averaging [5]. Such techniques are highly effective, can identify non-linearity in structures and are getting more and more popular. In general, modal identification techniques in time domain, however, need signals of higher quality. Modal identification techniques in time domain were applied in the study to measured signals on the Tsing Ma bridge.

Time-domain modal identification techniques use signals acquired simultaneously and need a large number of accelerometers and channels of data loggers for testing on large structures such as the Tsing Ma bridge. It is not practical to use hundreds of high-quality accelerometers and data logger channels to measure the structural health signature of the intact structure of the Tsing Ma bridge with 2160 m deck and 206 m towers. The measurement of the bridge responses, therefore, was forced to be divided into 15 groups because of the limited number of available high-quality accelerometers and data logger channels, with 13 groups for the deck and two groups for the two towers. Currently, there has been no published paper discussing identification of mode shapes of a complete bridge deck in time domain from data obtained group by group.

Eigensystem realization algorithms (ERA) are output-only time-domain modal identification techniques from free response signals. Unfortunately, the ambient responses of the Tsing Ma bridge are forced vibrations rather than free vibrations. Therefore, the ambient data should be transformed into free vibration data before usage of ERA. The random decrement technique (*RD*) is a good method to do this [6]. It defines, for instance, the simplest and classical *RD* function of an ambient signal $a(t)$ as

$$RD = \frac{1}{n} \sum_{i=1}^{v} a(t - t_i), \quad t \geqslant t_i,$$

where t_i, $i = 1, 2, \ldots, n$, is the time when $a(t)$ crosses down a fixed threshold λ, called triggering level, and t_i is called triggering point, see Figure 1. Such *RD* functions can be good

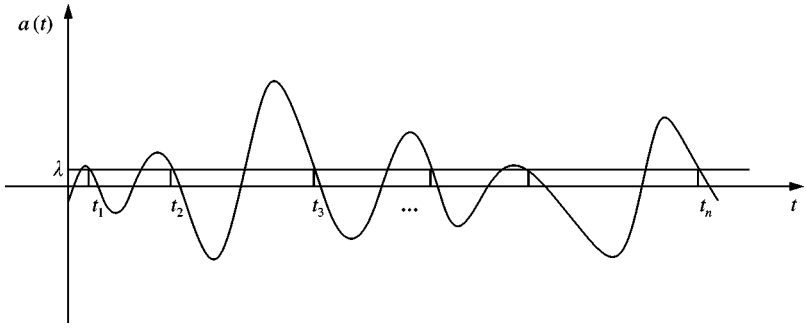

Figure 1. Calculation of random decrement function.

signatures. Besides, *RD* functions of ambient responses are proportional to the cross-correlation functions of the responses. The correlation operation plays the role of noise filtering.

An improved ERA, called fast ERA or FERA [7], was used in the paper to identify modes from the contaminated ambient data to obtain better modes. Differently from traditional ERA[8], FERA uses cross-correlation functions of *RD* functions instead of *RD* functions to build Hankel matrices and uses eigenvalue decomposition instead of singular value decomposition.

Fifteen groups of *RD* functions, as free response signals, were formed from the filtered ambient signals first. The modes of the Tsing Ma bridge were identified group by group. Then signals required at the reference measurement points were used to assemble modes of the complete bridge.

Software needed by all the calculations mentioned above for this identification was implemented by the authors. Then time-domain modal identification results are compared with respective analytical and frequency-domain modal identification results. The results show that the time-domain modal identification method is successful.

2. DESCRIPTION OF AMBIENT TEST

Ambient acceleration responses of the bridge were measured mainly in the vertical and transversal directions by servo-type accelerometers at 96 locations on the deck and towers. Acceleration signals at 170 degrees of freedom (d.o.f.) were divided into 15 groups with two sections. There were 13 d.o.f. in each group and signals were measured group by group due to the limited number of available Akashi V401 CR servo-type accelerometers with frequency band from 0 to 400 Hz and channels of TEAC R-280C FM data loggers. In each group, 10 different d.o.f. on the bridge and 3 d.o.f. at a "reference point" (one in each of vertical, longitudinal and transversal directions respectively) were measured simultaneously. Two reference points were selected for the bridge with the left reference point at section No. 15 and the right one at section No. 7. The left reference point was for the left part of the bridge and the right one was for the right part. The sampling rate of the data was 50 Hz and sampling lengths were 2 h for the deck, 1·5 h for the towers and 5 h for the two reference points. The cut-off frequency of the antialiasing filter was 20 Hz. Locations of the measured points are shown in Figures 2 and 3.

The weak ambient excitations without traffic loads and intensive excitations induced by the irregular and temporary movement of heavy construction vehicles led to a low ratio of

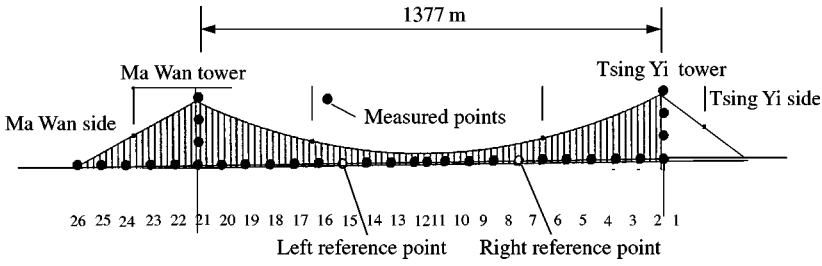

Figure 2. Measurement sections on Tsing Ma bridge.

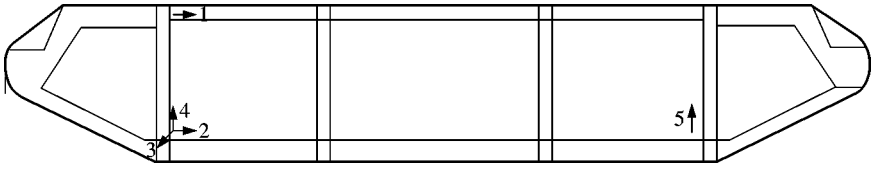

Figure 3. Layout of sensors on each measurement section.

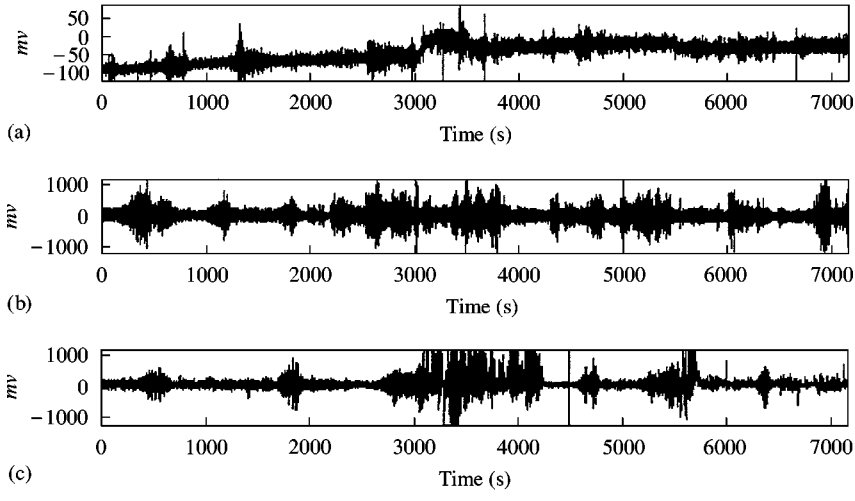

Figure 4. Examples of acquired signals of ambient acceleration responses of Tsing Ma bridge: (a) signal with zero-position offset/linearity (No. 5 in transverse direction of section 03/04); (b) signal with non-stationary/noise (No. 4 in vertical direction of section 15/16); and (c) signal with overflow/truncation (No. 5 in vertical direction of section 01/02).

signal to noise in the acquired responses. Besides, changes in wind speed (with lowest at 1·2 m/s and largest at 6·9 m/s) and changes in temperature (with lowest at 22°C and highest at 30°C) during the half-month testing often occurred even if it was not in typhoon season. In addition, some zero-position offset occurred in the data loggers that made some recordings have variable equilibrium positions. Therefore, the quality of the acquired data is poor. The data include zero position offset/linearity (see Figure 4(a)), non-stationarity/noise (see Figure 4(b)), and overflow/truncation (see Figure 4(c)). Some more pre-processing, such as delinearity and selection of relatively stationary segments, should be carried on before filtering.

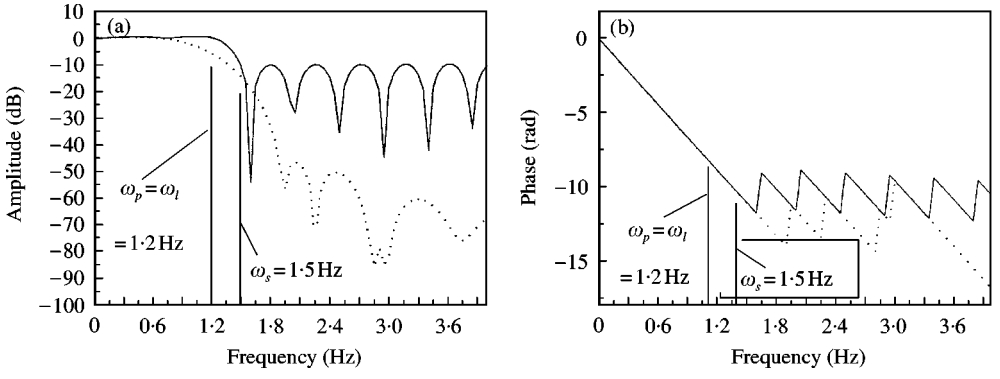

Figure 5. Comparison between Chebyshev filter and Hanning Window, (a) amplitude–frequency characteristic: ——, Chebyshev filter ; · · · · ·, Hanning window filter. (b) phase–frequency characteristic: ——, Chebyshev filter; · · · · ·, Hanning window filter.

3. DIGITAL SIGNAL FILTER

A digital filter with a Hanning window or others, which gave much less strict bandwidth (see Figure 5), was initially used for the work and the modal identification on so data filtered thus failed. The Chebyshev digital filter based on the Remez exchange algorithm [4] can specify accurately the edge frequencies of passband and stopband ω_p and ω_s, limit more strictly bandwidth and give filtering effect better than those by analogue and low-pass digital filters with different kinds of windows. Given ω_p, ω_s, δ_1 (ripple in passband) and δ_2 (attenuation in stopband), the filter frequency response function $H_r(\omega)$ satisfies the conditions

$$1 - \delta_1 \leqslant H_r(\omega) \leqslant 1 + \delta_1, \quad 0 \leqslant \omega \leqslant \omega_p,$$
$$- \delta_2 \leqslant H_r(\omega) \leqslant \delta_2, \quad \omega_s \leqslant \omega \leqslant \pi. \tag{1}$$

This study used the Chebyshev digital filter to replace digital filters with different kinds of windows for processing the initial signals. The edge frequencies were specified for the signals of the bridge: $\omega_p = 1{\cdot}2$ Hz, $\omega_s = 1{\cdot}5$ Hz for the stiffening deck because the first 40 analytical natural frequencies of the deck of the Tsing Ma bridge are in a range from 0·06 to 1·0 Hz; $\omega_p = 6{\cdot}5$ Hz, $\omega_s = 7$ Hz for the towers because the first 30 analytical natural frequencies of the towers of the Tsing Ma bridge are in a range from 0·39 to 6·2 Hz. The sections as stationary as possible in the original signals should be selected for processing. As an example, a more stationary section from 600 to 6000 s of the original recording as shown in the left figure of Figure 6(a) was selected and the section after filtering is shown in the left figure of Figure 6(b). Comparison between the auto-power spectrum of the original data (see the right of Figure 6(a)) and the auto-power spectrum of the filtered data (see the right figure of Figure 6(b)), shows the direct components, linearity offsets and frequency components in the range above 1·2 Hz in the filtered data are completely removed. The quality of modal identification with these well-filtered vibration data was improved and the identification efficiency was also greatly improved.

4. TIME-DOMAIN MODAL IDENTIFICATION

Many time-domain modal identification techniques from output-only data have been developed, such as ITD, auto-regressive moving average models (ARMA), polyreference

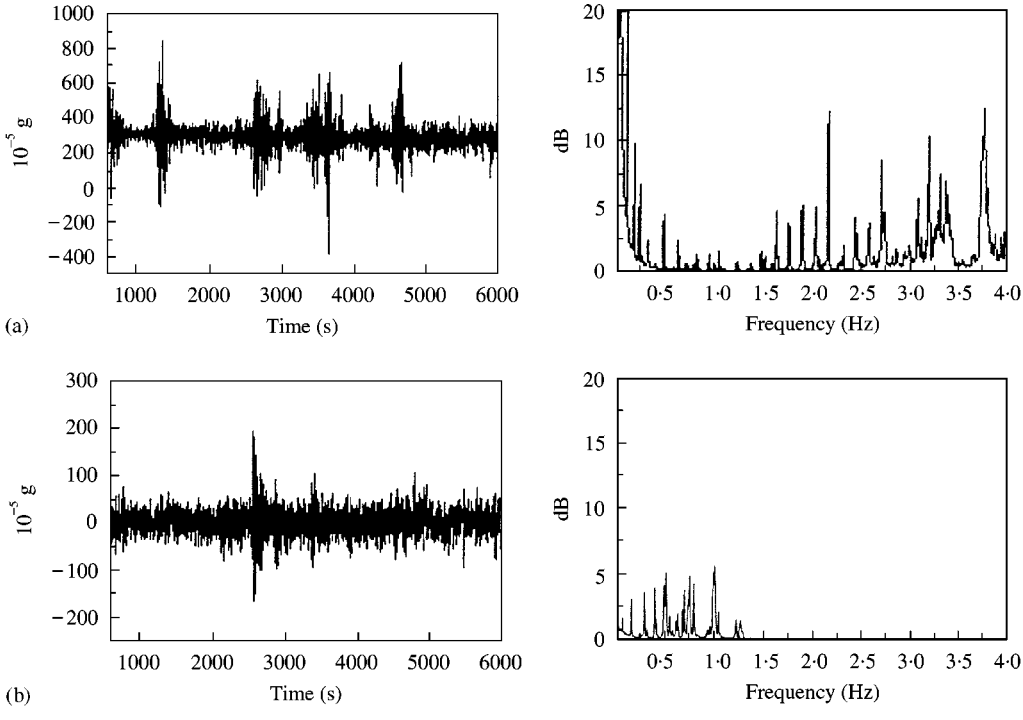

Figure 6. Comparison between original data and filtered data of bridge deck. (a) Time Waveform and its Auto Power Spectrum of original data of bridge deck. (b) Time Waveform and its Auto Power Spectrum of filtered data with Chebyshev filter of bridge deck.

least-squares complex exponential (LSCE), ERA method, stochastic subspace method and so on [9, 10].

The noises and non-stationarity in the acquired data caused by the irregular movement of construction vehicles have similar frequency contents as those of ambient responses. There is no quantitative indication for ratios of signal to such noises in the data. It is difficult to completely cleanse such contaminated data by filtering. Initially, ITD technique was used to identify modes from such filtered data, but failed. A more effective modal identification method is necessary to identify modes from such data.

FERA has two improvements on ERA. The first improvement is using the cross-correlation matrices of *RD* functions to replace *RD* functions for building Hankel matrices, that is another filtering, for which a brief explanation is given in the next section of the paper. This may be the main reason that FERA can produce better results of modal identification from seriously contaminated data than ERA does. The second improvement is using eigensystem decomposition to replace singular value decomposition, a very time-consuming algorithm. In general, this makes FERA 5–10 times more effective than ERA. In this work, FERA had the capacity to manage modes as many as needed. In order to reduce the influence from noises, FERA was employed in the paper for modal identification.

4.1. MODAL IDENTIFICATION PROCEDURE

Mode identification of the complete Tsing Ma bridge was carried out in the following three steps.

(1) *Calculation of RD functions*: The original signals are ambient responses. It is necessary to convert the forced vibration signals to free responses—*RD* function matrices $\mathbf{Y}(i)$. In order to reduce furthermore noises in *RD* functions, triggering points to each recording should be as many as possible, which requires lower triggering levels. However, in order to obtain a high ratio of signal to noise in the *RD* functions, each *RD* function should have values as large as possible, which required higher triggering levels. The two contradictory requirements led to a compromised choice that lengths of the producedd *RD* functions were determined as 4096 points (81·92 s) for the stiffening deck and 2048 or 1024 points for the towers. To keep the numbers of triggering points for every recording between 1000 and 2000, different triggering levels were selected for different measured data groups.

(2) *Identification of mode group by group using FERA*: At first, the cross-correlation matrix of *RD* functions was evaluated as

$$\mathrm{R}(q) = \frac{1}{\mathrm{r}} \sum_{i=1}^{r} \mathbf{RD}(q+i)\mathbf{RD}^{\mathrm{T}}(i), \tag{2}$$

which is an averaging operation suppressing random noises, and also called correlation filtering. Figure 7(a) and 7(b) compare the effect of correlation filtering. The cross-correlation matrix was used to establish the Hankel matrix

$$\mathbf{U} = \begin{bmatrix} \mathbf{R}(0) & \mathbf{R}(1) & \cdots & \mathbf{R}(\beta-1) \\ \mathbf{R}(1) & \mathbf{R}(2) & \cdots & \mathbf{R}(\beta) \\ \cdots & \cdots & \cdots & \cdots \\ \mathbf{R}(\alpha-1) & \cdots & \cdots & \mathbf{R}(\alpha+\beta-2) \end{bmatrix}_{\alpha S \times \beta S}, \tag{3}$$

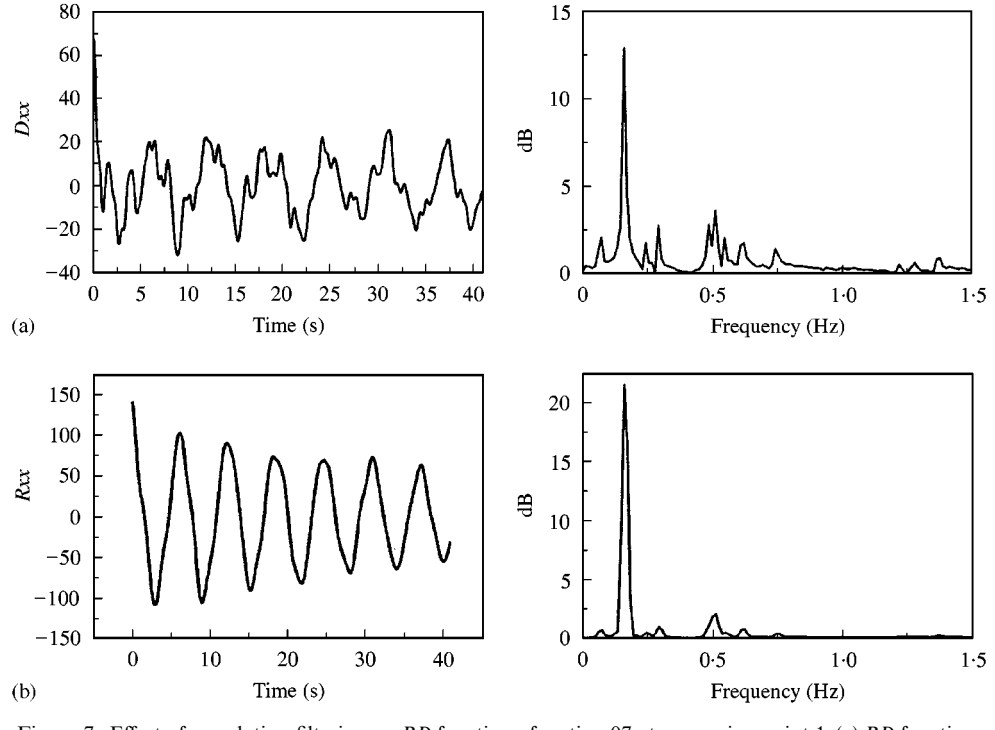

Figure 7. Effect of correlation filtering on *RD* function of section 07 at measuring point 1: (a) *RD* function and its power spectrum, (b) auto-correction function of *RD* function and its power spectrum.

where integers α and β are important for accuracy of modal identification. In general,

$$(\alpha + \beta)/(4m) < s \quad \text{and} \quad \alpha > \beta,$$

where m being the number of measurement points, and s the length of data.

A matrix $\mathbf{S} = \mathbf{U}\mathbf{U}^{\mathrm{T}}$ was built. Then eigenvalue decomposition of $\mathbf{S}$

$$\mathbf{S} = \mathbf{P}\mathbf{D}\mathbf{P}^{\mathrm{T}} = \mathbf{V}\mathbf{V}^{\mathrm{T}} \tag{4}$$

was performed to obtain the system eigenvector matrix $\mathbf{V}$ and the eigenvalue matrix $\mathbf{D}$, from which the modes of the Tsing Ma bridge were determined. The following example shows the efficiency of eigenvalue decomposition. For a structure with 10 d.o.f. with five measurement points and five impulsive excitation points, and with a selection of $\alpha = \beta = 40$, FERA is 4·6 times faster than ERA. The more the d.o.f., α or β, the faster is FERA than ERA.

Some indices can be used to delete false modes. For instance, the mode confidence factor (MCF) [12] is defined as

$$MCF_r = \left| \frac{\bar{p}_{kr}}{p_{kr} \mathrm{e}^{s_r \Delta t}} \right|, \tag{5}$$

where p_{kr} is the kth component (not at modal nodes, and the larger its value, the better) of the rth mode shape identified from contaminated data, $\bar{p}_{kr}$ identified above from the same data but with a time delay Δt, s_r the rth eigenvalue. An identified mode with $MFC = 1{\cdot}0$ will be a certainly true mode. Another index, the mode assurance criteria (MAC) can also be used to delete false modes.

(3) *Assembling modes of the complete bridge*: After 15 groups of mode pieces were identified by using FERA, assembling modes was carried out. The assembling work consisted of three stages: (1) Unify natural frequencies—pre-assemble pieces of mode shapes of different groups with very closed frequencies to conform whether they belong to the same mode. If it is the case, each of the true natural frequencies was taken as the average of the closed frequencies of all different groups. (2) Assembling mode shapes—assemble the right half of the complete bridge using data acquired at the right reference point and assemble the left half using data acquired at the left reference point, and then assemble mode shapes of the complete bridge using the data at the two reference points. (3) Modal damping ratios were determined only from the signals acquired at section 11/12 which are of the best quality.

The assembling procedure is as follows. Assuming that a mode shape is being assembled and that the ith pieces of the mode shape ($i = 1, 2, \ldots, 12$) of the ith deck section belonging to the right half of the bridge is denoted by $\boldsymbol{\Psi}_{ir}$, the mode shape of the right half deck including six groups are

$$\begin{Bmatrix} 1 \\ \boldsymbol{\Psi}_{1r} \\ \boldsymbol{\Psi}_{2r} \end{Bmatrix}, \quad \begin{Bmatrix} 1 \\ \boldsymbol{\Psi}_{3r} \\ \boldsymbol{\Psi}_{4r} \end{Bmatrix}, \ldots, \begin{Bmatrix} 1 \\ \boldsymbol{\Psi}_{11r} \\ \boldsymbol{\Psi}_{12r} \end{Bmatrix},$$

where each bracket is the mode shape pieces of one group belonging to the right half deck and includes mode pieces of two sections and a component at the right reference point which is normalized to unit. Each section includes five points, see Figure 3. The mode shapes of the right half can be determined from the above equation as

$$\boldsymbol{\Psi}_r = \{\boldsymbol{\Psi}_{1r}^{\mathrm{T}} \boldsymbol{\Psi}_{2r}^{\mathrm{T}} \cdots \boldsymbol{\Psi}_{6r}^{\mathrm{T}} \ \ 1 \ \ \boldsymbol{\Psi}_{8r}^{\mathrm{T}} \cdots \boldsymbol{\Psi}_{13r}^{\mathrm{T}}\}^{\mathrm{T}}. \tag{6}$$

Similarly, the mode shapes of the left half can be determined by

$$\mathbf{\Psi}_l = \{\mathbf{\Psi}_{1l}^{\mathrm{T}}\mathbf{\Psi}_{2l}^{\mathrm{T}} \cdots \mathbf{\Psi}_{6l}^{\mathrm{T}} \;\; 1 \;\; \mathbf{\Psi}_{8l}^{\mathrm{T}} \cdots \mathbf{\Psi}_{13l}^{\mathrm{T}}\}^{\mathrm{T}}. \tag{7}$$

Then the signals acquired at the two reference points

$$\mathbf{\Psi} = \begin{Bmatrix} \mathbf{\Psi}_r \\ \mathbf{\Psi}_l \end{Bmatrix} \tag{8}$$

were used to combine equations (6) and (7), that led to the modes of the complete bridge.

$$\{\mathbf{\Phi}_{1l}^{\mathrm{T}}\mathbf{\Phi}_{2l}^{\mathrm{T}} \cdots \mathbf{\Phi}_{13l}^{\mathrm{T}}\mathbf{\Phi}_{1r}^{\mathrm{T}}\mathbf{\Phi}_{2r}^{\mathrm{T}} \cdots \mathbf{\Phi}_{13r}^{\mathrm{T}}\}^{\mathrm{T}}. \tag{9}$$

The differences between phase angles at measured points and at the reference point in any group were used to assemble mode shapes. Any phase difference staying in between plus and minus 15° was set to 0°, and phase differences staying in between a 165 and a 195° was set to a 180°. Other phase differences showed complex modes [12].

4.2. RESULTS OF MODAL IDENTIFICATION

Seventy-nine modes were identified, including 35 modes with each mode shape identified at 26 points and with straight line segments to join neighboring points for the stiffening deck (including 17 lateral bending modes LD, eight longitudinal bending modes LT and five torsional modes TD), 26 modes with each mode shape identified at 10 points and with straight line segments to join neighbor points for the Tsing Yi tower (including 10 lateral bending modes ST, 13 longitudinal bending modes LT and five torsional modes TT) and 18 modes for the Ma Wan tower (including seven lateral bending modes ST, six longitudinal bending modes LT and five torsional modes TT). Five modes among the 79 identified modes are complex modes. Figure 19 shows that the mode shape components at the two towers have about 90° difference of phase angles in comparison with other deck components. Existence of the complex modes is reasonable because damping in the two towers are different from damping in the deck. It is not difficult to derive normal modes from complex modes [13].

Tables 1, 2 and 3 compare the identified frequencies and damping ratios of lateral bending, vertical bending and torsional modes of the deck with finite element analytical results and results identified by using frequency-domain techniques [14, 15] respectively. The transverse mode LD8 of the deck and torsional mode TD3 of the deck are coupled, and the transverse mode LD16 of the deck and torsional mode TD6 of the deck are coupled. Tables 4, 5 and 6 compare the identified frequencies and damping ratios of lateral bending, longitudinal bending and torsional modes of the two towers respectively. The transverse mode ST12 of the Tsing Yi tower and torsional mode TT7 of the Tsing Yi tower are coupled, the longitudinal mode LT3 of the Tsing Yi tower and Ma Wan tower and vertical mode VD13 of the deck are coupled and the lateral mode LD6 of the deck and lateral mode ST1 of the Tsing Yi tower are coupled.

Figures 8, 9 and 10 compare the first, second and 15th lateral bending mode shapes of the deck respectively. Figures 11, 12 and 13 compare the identified first, fourth and 12th vertical bending modes of the deck respectively. Figures 14, 15 and 16 compare the identified first, third and sixth torsional modes of the deck respectively. Figures 17 and 18 compare the identified first lateral bending mode of the Tsing Yi tower and second lateral bending mode of the Ma Wan tower respectively. Other mode shapes are not shown here due to limited space.

TABLE 1

Frequencies and damping ratios of lateral bending modes of deck

	Frequency (Hz)			Damping ratio (%)	
Mode	Analytical	FRF	FERA	FRF	FERA
LD1	0·062	0·069	0·069	0·89	0·840
LD2	0·138	0·161	0·161	0·50	0·936
LD3	0·232	0·242	—	0·21	—
LD4	0·241	0·246	0·245	0·16	0·367
LD5	0·365	0·293	0·292	0·26	0·616
LD6	0·393	0·391	0·394	0·46	0·892
LD7	0·409	0·408	—	—	—
LD8	0·452	0·490	0·488	—	0·290
LD9	0·547	0·548	0·548	0·32	0·153
LD10	0·568	0·578	0·577	—	0·384
LD11	—	0·616	0·612	—	0·670
LD12	0·670	0·677	0·673	—	0·332
LD13	0·692	0·698	0·697	0·12	0·285
LD14	0·740	0·735	0·729	0·11	0·810
LD15	0·756	0·748	0·749	—	0·514
LD16	0·814	0·773	0·792	—	0·215
LD17	0·856	0·839	0·831	0·11	0·449
LD18	0·898	0·931	0·935	—	0·405
LD19	0·983	1·008	0·992	—	0·992

TABLE 2

Frequencies and damping ratios of vertical bending modes of deck

	Frequency (Hz)			Damping ratio (%)	
Mode	Analytical	FRF	FERA	FRF	FERA
VD1	0·112	0·114	0·114	0·96	0·687
VD2	0·134	0·137	0·137	0·62	1·040
VD3	0·180	0·183	0·183	0·62	0·343
VD4	0·234	0·240	0·240	0·33	0·339
VD5	0·276	0·281	0·281	0·20	0·318
VD6	0·321	0·326	0·325†	—	0·621
VD7	0·398	0·404	0·401	0·11	0·140
VD8	0·492	0·497	0·494†	0·12	0·270
VD9	0·587	0·591	0·591	0·20	0·240
VD10	0·726	0·715	0·712	0·21	0·240
VD11	0·847	0·828	0·826	0·14	0·204
VD12	0·972	0·949	0·947	—	0·243
VD13	0·996	1·060	1·062	—	0·346

†Complex modes

Figures 8 and 9 show that the lateral bending modes LD1 and LD2 identified by FERA have two peaks at sections 6–8 and 14–16 and that the peaks of LD1 are much higher than the mode components here identified by FRF. This is because the days when the two sections were measured had the highest wind speed (6·9 m/s) with relatively strong

TABLE 3

Frequencies and damping ratios of torsional modes of deck

Mode	Frequency (Hz)			Damping ratio (%)	
	Analytical	FRF	FERA	FRF	FERA
TD1	0·250	0·265	0·265	0·27	0·200
TD2	0·258	0·320	0·322	0·33	1·257
TD3	0·476	0·485	0·485	—	0·553
TD4	0·531	0·591	—	—	—
TD5	0·652	0·633	0·635	—	0·294
TD6	0·654	0·791	0·794	—	0·255
TD7	0·880	0·883	—	—	—

TABLE 4

Frequencies and damping ratios of lateral bending modes of towers

	Tsing Yi tower				Ma Wan tower			
	Frequency (Hz)		Damping ratio (%)		Frequency (Hz)		Damping ratio (%)	
Mode	FRF	FERA	FRF	FERA	FRF	FERA	FRF	FERA
ST1	0·391	0·400	0·580	2·027	—	—	—	—
ST2	0·520	0·529	0·640	4·719	0·438	0·413	—	3·720
ST3	0·551	—	0·510	—	0·492	0·506	—	3·872
ST4	0·598	—	0·380	—	0·516	—	—	—
ST5	1·043	1·075	—	0·631	—	1·053	—	2·350
ST6	1·426	1·436	0·540	3·396	1·219	—	—	—
ST7	1·461	1·450	0·540	1·330	1·282	1·257	—	4·245
ST8	1·544	1·550	—	0·230	—	—	—	—
ST9	1·704	1·754	0·230	1·871	—	1·666	—	0·681
ST10	2·227	2·267	0·370	1·946	1·977	1·977	—	1·579
ST11	3·838	3·845	0·380	0·787	2·427	2·443	—	1·311
ST12	4·056	4·035	0·330	0·354	—	—	—	—

non-stationarity. The significantly non-stationary ambient response recordings of these two sections made it difficult to find stationary segments long enough to build *RD* functions with good quality for the two sections. Relatively stronger ambient responses led to that much larger triggering levels being used when the *RD* functions were determined for these two sections. In addition, according to the recordings of wind speed at Tsing Ma bridge [16] wind power spectra had maximum values at about 0·03 Hz with the value at 0·069 Hz, the frequency of LD1, being 7 times as large as that at 0·161 Hz, the frequency of mode LD2. Therefore, the LD1 mode shapes identified by using FERA together with *RD* are influenced more strongly by the gusts than the other modes.

The results of modal identification of the Tsing Ma bridge in this work, were compared with finite element analytical results and results given by frequency response function method (FRF). The comparison shows good agreement in the identified frequencies and mode shapes, except for a few mode shapes.

TABLE 5

Frequencies and damping ratios of longitudinal bending modes of towers

	Tsing Yi tower				Ma Wan tower			
	Frequency (Hz)		Damping ratio (%)		Frequency (Hz)		Damping ratio (%)	
Mode	FRF	FERA	FRF	FERA	FRF	FERA	FRF	FERA
LT1	0·645	—	0·580	—	0·648	0·638	0·420	1·786
LT2	0·730	0·723	—	0·447	—	—	—	—
LT3	1·069	1·075	0·450	0·278	1·059	1·108	—	1·814
LT4	1·547	1·534	0·560	0·838	1·527	1·527	0·510	0·784
LT5	2·027	2·036	—	0·291	2·036	2·105	0·390	1·617
LT6	2·113	2·112	—	1·164	—	—	—	—
LT7	2·305	2·205	—	0·518	2·947	2·947	—	0·511
LT8	2·805	2·780	—	0·367	—	—	—	—
LT9	2·934	2·932	—	2·260	—	—	—	—
LT10	5·746	—	—	—	5·666	5·668†	—	0·548

†Complex modes

TABLE 6

Frequencies and damping ratios of torsional modes of towers

	Tsing Yi tower				Ma Wan tower			
	Frequency (Hz)		Damping ratio (%)		Frequency (Hz)		Damping ratio (%)	
Mode	FRF	FERA	FRF	FERA	FRF	FERA	FRF	FERA
TT1	0·883	0·891	0·440	1·478	0·883	0·888	0·430	1·861
TT2	1·333	—	0·260	—	1·336	—	—	—
TT3	1·883	1·882	—	0·216	1·879	1·894	—	0·595
TT4	1·914	1·916	—	0·619	—	—	—	—
TT5	2·422	2·404	—	0·734	2·542	2·540	—	0·172
TT6	3·300	3·256†	—	0·707	3·298	3·258†	0·330	1·032
TT7	4·069	4·077	—	0·610	3·744	3·752	0·420	0·435
TT8	4·203	4·194	—	0·516	—	—	—	—
TT9	6·207	5·381	—	0·390	—	—	—	—

†Complex modes

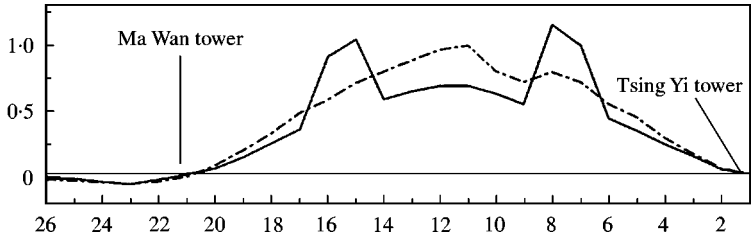

Figure 8. Lateral bending mode of deck-LD1: ——, FERA; – · –, FRF.

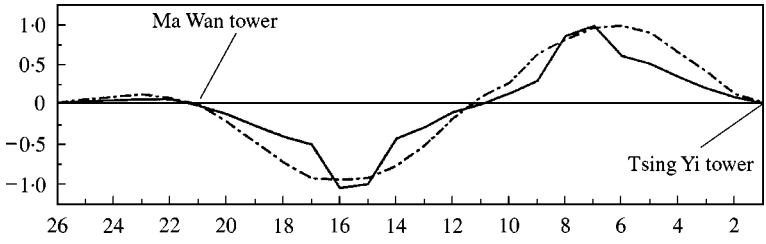

Figure 9. Lateral bending mode of deck-LD2: ——, FERA; – · –, FRF.

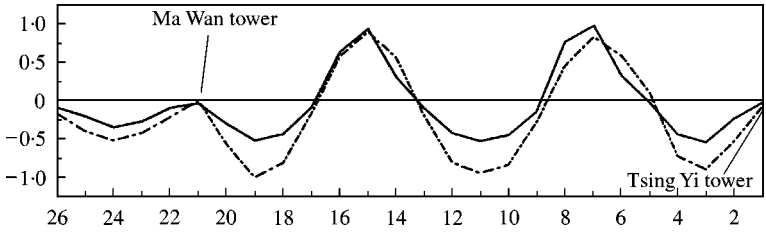

Figure 10. Lateral bending mode of deck-LD15: ——, FERA; – · – ·, FRF.

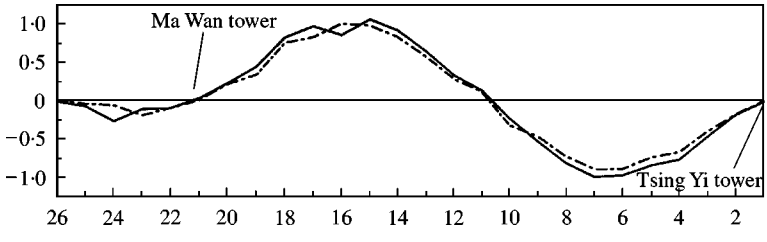

Figure 11. Vertical bending mode of deck-VD1: ——, FERA; – · – · –, FRF.

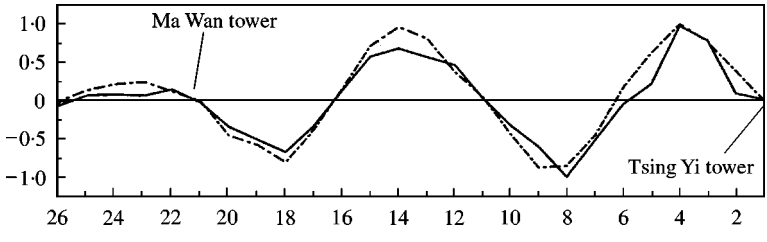

Figure 12 Vertical bending mode of deck-VD4: ——, FERA; – · –, FRF.

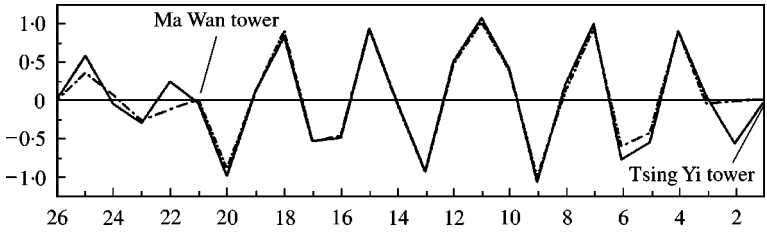

Figure 13. Vertical bending mode of deck-VD12: ——, FERA; – · –, FRF.

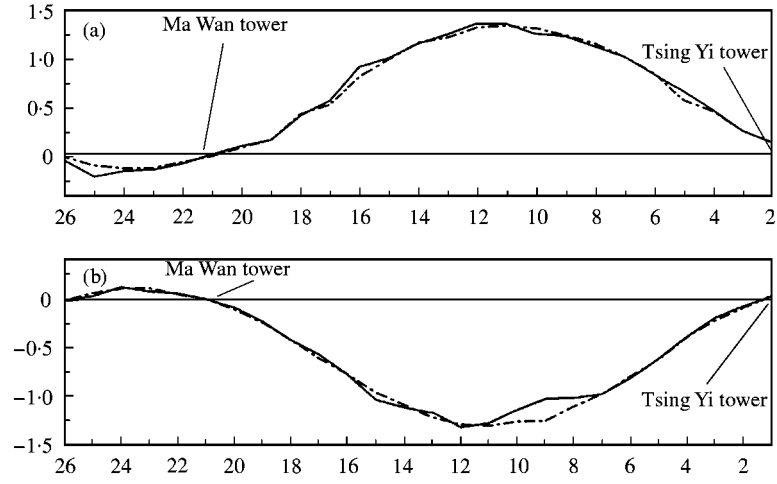

Figure 14. Torsional mode of deck-TD1: (a) At south truss: ——, FERA; – · –, FRF. (b) At north truss: ——, FERA; – · –, FRF.

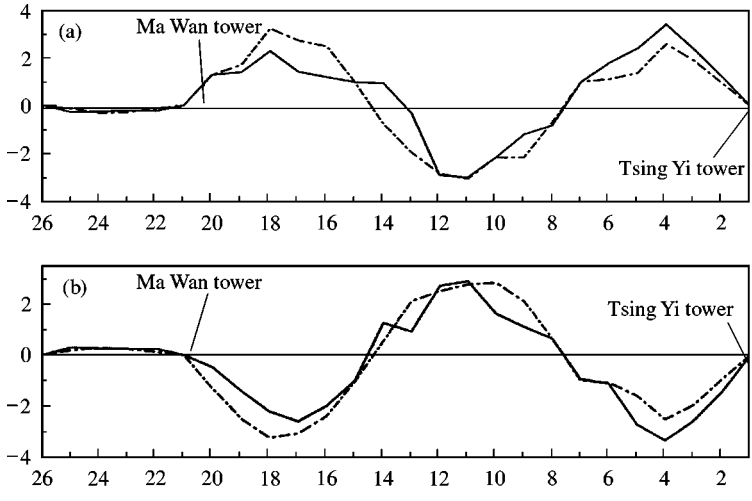

Figure 15. Torsional mode of deck-TD3: (a) At south truss: ——, FERA; – · –, FRF. (b) At north truss: ——, FERA; – · –, FRF.

Since FRF assumes that resonance response occurs at only one mode and identifies modal parameters by peak-picking, the identification precision is greatly affected by the ratio of frequency resolution to half-power point bandwidth of spectral peak. Many modal damping ratios could not be identified by using FRF and the damping ratios identified in frequency domain are not dependable. However, FERA was used with *RD* functions produced from well-filtered data, the noise effect was greatly reduced and false modes were also greatly reduced. A study on the errors in these identified modes and the sensitivities of these identified modes to noise, a difficult work, is being carried out.

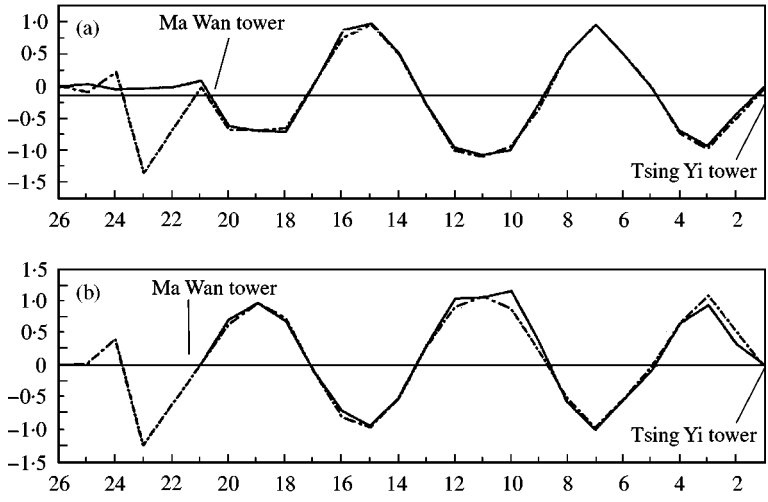

Figure 16. Torsional mode of deck-TD6: (a) At south truss: ——, FERA; – · –, FRF. (b) At north truss: ——, FERA; – · –, FRF.

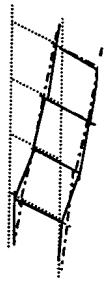

Figure 17. First Lateral bending mode of Tsing Yi tower: ——, FERA, – · –, FRF.

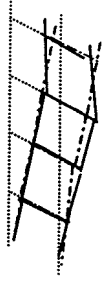

Figure 18. Second Lateral bending mode of Ma Wan tower: ——, FERA, – · –, FRF.

5. CONCLUSION

1. In order to cut off the noise from the test data and to obtain stationary vibration signals, it is necessary to design a suitable digital filter and to choose the passband and stopband edge frequencies correctly before modes were identified. The Chebyshev digital filter has been used in this study instead of digital filters with a Hanning window or others because it can strictly define the passband and stopband edge frequencies. The results show

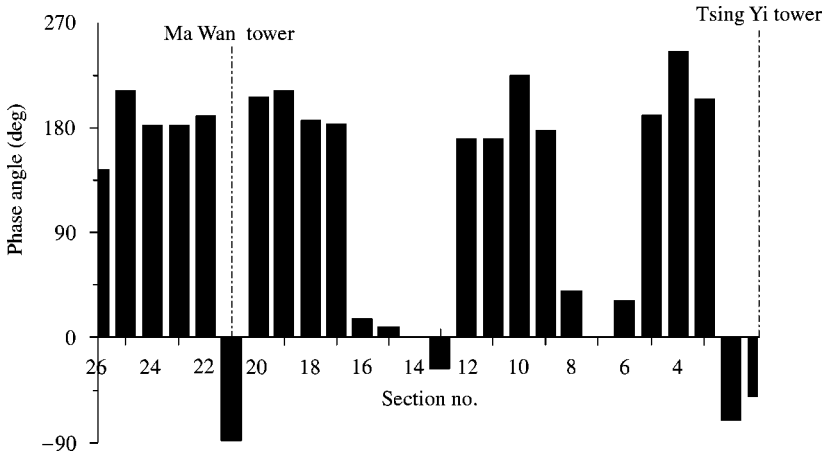

Figure 19. Phase results of vertical bending complex mode of deck-VD6.

that it will give better filtering effects than that given by digital filters with the windows and analogue filters.

2. For the establishment of *RD* functions of the filtered signals, it is necessary to transform the ambient response signals into free responses before the usage of FERA. To deal with differences in testing situations for various groups, different triggering levels should be selected for different groups of recordings. As a result, different *RD* functions will have nearly the same numbers of triggering points and good *RD* functions can then be obtained.

3. FERA method uses cross-correlation function matrix of *RD* functions instead of *RD* functions to form the Hankel matrix and uses eigenvalue decomposition instead of singular value decomposition to identify modes. Consequently, it has a better capacity to process contaminated signals and has higher computation efficiency. The identified results show that the FERA method is a good output-only identification method in time domain.

4. The bridge modes were identified group by group. Assembling mode pieces to form complete modes was necessary after the mode pieces of all groups were identified. The relationships between the different reference points and other measurement points can be used to combine the modes of the complete bridge. Comparison of the modes identified in the study with the analytical modes and the results identified by using the frequency-domain technique shows that the modal identification method in this paper is successful but with the exception of a few mode shapes which are not as good.

ACKNOWLEDGMENTS

The authors express their gratitude to the National Key Research Project "Climbing B" of the China Ministry of Science and Technology and the Highways Department of the Government of Hong Kong SAR for the financial support of the study.

REFERENCES

1. Q. QIN and W. ZHANG 1998 *Proceedings of IMAC* XVI, *Santa Barbara, U.S.A., February* 2–5, 945–951. Damage detection of suspension bridges.

2. K. Y. WONG, C. K. LAU and K. C. YEUNG 1995 *Proceedings of Bridges into the* 21*st Century*, *Hong Kong*, *October*, 539–548. Wind and structural health monitoring system (WASHMS) for Lantau fixed crossing (Part I, system planning and design).
3. A. M. ABDEL-GHAFFAR and R. H. SCANLAN 1985 *Journal of Engineering Mechanics* **111**, 907–924. Ambient vibration studies of Golden Gate Bridge: I. Suspended structure.
4. T. W. PARKS and C. S. BURRUS 1987 *Digital Filter Design*. NY: U.S.A.: John Wiley & Sons.
5. P. ANDERSEN, R. BRINCKER, B. PEETERS, G. DE ROECK and L. HERMANS 1999 *Proceedings of IMAC* XVII, *Orlando*, *FL*, *U.S.A*., 1035–1041. Comparison of system identification methods using ambient bridge test data.
6. J. C. ASMUSSEN 1997 *Ph.D. Thesis*, *Aalborg University*, *Denmark*. Modal analysis based on the random decrement technique application to civil engineering structures.
7. F. Q. LIU and L. M. ZHANG 1999 *Journal of Vibration Engineering* **12**, 316–322. An improved eigensystem realization algorithm and its application to modal parameter identification of intelligent space trusses. (in Chinese).
8. T. SIMMERMACHER, M. KAOUK and D. C. ZIMMERMAN 1997 *Proceedings of IMAC* XV, *Orlando*, *FL*, *U.S.A*., 914–921. Exploiting aliasing effects in the eigensystem realization algorithm.
9. L. M. ZHANG and F. Q. LIU 1998 *Research Report of China National Key* '*Climbing B*' *Project*, *Beijing*. Statistical research on modal identification techniques in time domain. (in Chinese).
10. Z. F. FU 1990 *Vibration Model Analysis and Parameters Identification*. Beijing, China: Publishing Company of Mechanical Industry (in Chinese).
11. R. S. PAPPA and S. R. IBRAHIM 1981 *Shock and Vibration Bulletin* **51**, 43–72. A parametric study of the time domain modal identification algorithm.
12. D. B. LI 1987 *Journal of Tsinghua University* **27**, 86–94. Understanding of several problems in modal analysis (in Chinese).
13. S. R. IBRAHIM 1983 *American Institute of Aeronautics and Astronautics Journal* **21**, 446–451. Computation of normal modes from measured complex modes.
14. Highways Department, Hong Kong 1991 *Report* 113, Flint & Neill Partnership, *June*. Lantau fixed crossing, independent appraisal of the design of Tsing Ma bridge.
15. X. L. LIU and Q. QIN 1999 *Report of Department of Civil Engineering*, *Tsinghua University*. The dynamic testing/measurement on complete Tsing Ma bridge after the completion of pavement surface.
16. C. K. LAU and K. Y. WONG 1999 *Report of Highways Department*, *Hong Kong SAR*. Primary monitoring results of Tsing Ma bridge.